 CMES, vol.37, no.3, pp.274-304, 2008

A Variational Formulation of a Stabilized Unsplit Convolutional Perfectly Matched Layer for The Isotropic or Anisotropic Seismic Wave Equation

R. Martin[1], **D. Komatitsch**[1,2] **and S. D. Gedney**[3]

Abstract: In the context of the numerical simulation of seismic wave propagation, the perfectly matched layer (PML) absorbing boundary condition has proven to be efficient to absorb surface waves as well as body waves with non grazing incidence. But unfortunately the classical discrete PML generates spurious modes traveling and growing along the absorbing layers in the case of waves impinging the boundary at grazing incidence. This is significant in the case of thin mesh slices, or in the case of sources located close to the absorbing boundaries or receivers located at large offset. In previous work we derived an unsplit convolutional PML (CPML) for staggered-grid finite-difference integration schemes to improve the efficiency of the PML at grazing incidence for seismic wave propagation. In this article we derive a variational formulation of this CPML method for the seismic wave equation and validate it using the spectral-element method based on a hybrid first/second-order time integration scheme. Using the Newmark time marching scheme, we underline the fact that a velocity-stress formulation in the PML and a second-order displacement formulation in the inner computational domain match perfectly at the entrance of the absorbing layer. The main difference between our unsplit CPML and the split GFPML formulation of Festa and Vilotte (2005) lies in the fact that memory storage of CPML is reduced by 35% in 2D and 44% in 3D. Furthermore the CPML can be stabilized by correcting the damping profiles in the PML layer in the anisotropic case. We show benchmarks for 2D heterogeneous thin slices in the presence of a free surface and in anisotropic cases that are intrinsically unstable if no stabilization of the PML is used.

Keyword: Perfectly matched layers, Spectral elements, Boundary conditions,

[1] Université de Pau et des Pays de l'Adour, CNRS and INRIA Magique-3D. Laboratoire de Modélisation et Imagerie en Géosciences UMR 5212, Avenue de l'Université, 64013 Pau cedex, France. E-mail:roland.martin@univ-pau.fr, dimitri.komatitsch@univ-pau.fr

[2] Institut universitaire de France, 103 boulevard Saint-Michel, 75005 Paris, France.

[3] Department of Electrical and Computer Engineering, University of Kentucky, Lexington, KY 40506-0046, USA. E-mail:gedney@engr.uky.edu

Wave propagation.

1 Introduction

In the last decades, significant efforts have focused on developing efficient numerical tools to simulate seismic wave propagation in complex geological structures. Some commonly used numerical techniques are the finite-difference method (e.g., Alterman and Karal, 1968; Madariaga, 1976), spectral and pseudo-spectral techniques (e.g., Tessmer and Kosloff, 1994; Carcione, 1994), boundary-element or boundary-integral methods (e.g., Kawase, 1988; Sánchez-Sesma and Campillo, 1991; Rodríguez-Castellanos, Sánchez-Sesma, Luzón, and Martin, 2006; Abreu, Mansur, Soares-Jr, and Carrer, 2008), finite-element methods (e.g., Lysmer and Drake, 1972; Bao, Bielak, Ghattas, Kallivokas, O'Hallaron, Shewchuk, and Xu, 1998; Soares-Jr, Mansur, and Lima, 2007) and spectral-element methods (e.g., Komatitsch and Vilotte, 1998; Komatitsch and Tromp, 1999; Komatitsch, Martin, Tromp, Taylor, and Wingate, 2001). Recently, immersed interface techniques and discontinuous Galerkin formulations related to discontinuity-capturing finite-volume methods have also been developed (e.g., Dumbser and Käser, 2006).

Besides, a wide variety of absorbing layer techniques have also been developed and adapted to the above mentioned techniques in order to achieve almost no spurious numerical reflections at the outer boundaries of the computational domain and efficiently simulate unbounded media at the local or regional scale: damping layers or 'sponge zones' (e.g., Cerjan, Kosloff, Kosloff, and Reshef, 1985; Sochacki, Kubichek, George, Fletcher, and Smithson, 1987), paraxial conditions (e.g., Engquist and Majda, 1977; Clayton and Engquist, 1977; Stacey, 1988; Higdon, 1991), optimized conditions (e.g., Peng and Töksoz, 1995), the eigenvalue decomposition method (e.g., Dong, She, Guan, and Ma, 2005), continued fraction absorbing conditions (e.g., Guddati and Lim, 2006), exact absorbing conditions on a spherical contour (e.g., Grote, 2000), or asymptotic local or non-local high-order operators (e.g., Givoli, 1991, 2004, 2008; Hagstrom and Hariharan, 1998; Hagstrom, 1999). But at grazing incidence the local conditions produce spurious low frequency energy reflected off the boundaries at all angles of incidence, sponge layers require a very large number of grid points in the layer, paraxial conditions do not absorb efficiently waves impinging the boundaries at grazing incidence and may become unstable for values of Poisson's ratio greater than typically 2.

As explained for instance in Komatitsch and Martin (2007), the PML, introduced by Bérenger (1994) for Maxwell's equations, can overcome these drawbacks. It has the advantage of having a zero reflection coefficient at all angles of incidence and at all frequencies before discretization by a numerical scheme. It was rapidly reformulated with complex coordinate stretching for a split wave field (e.g., Chew and

Weedon, 1994; Collino and Monk, 1998) and applied to acoustic (e.g., Lu and Zhu, 2007) and elastic problems (e.g., Chew and Liu, 1996; Collino and Tsogka, 2001; Fauqueux, 2003; Komatitsch and Tromp, 2003; Cohen and Fauqueux, 2005; Festa and Vilotte, 2005; Ma and Liu, 2006; Komatitsch and Martin, 2007; Basu, 2009) as well as to poroelastic media (e.g., Zeng, He, and Liu, 2001; Martin, Komatitsch, and Ezziani, 2008). In the context of finite-difference formulations of the classical PML, the seismic wave equation is usually formulated as a first-order velocity-stress system in time. This formulation can not be used as such in second-order displacement formulations such as finite-element methods (e.g., Bao, Bielak, Ghattas, Kallivokas, O'Hallaron, Shewchuk, and Xu, 1998), spectral-element methods (e.g., Komatitsch and Vilotte, 1998; Komatitsch and Tromp, 1999; Komatitsch, Martin, Tromp, Taylor, and Wingate, 2001), and some finite-difference methods (e.g., Moczo, Kristek, and Bystrický, 2001). Komatitsch and Tromp (2003) and Basu and Chopra (2004) derived PML formulations suitable for the second-order system written in displacement and Festa and Vilotte (2005) showed that the first-order PML formulation can be used together with a second-order formulation of the equations inside the computational domain because the Newmark time-stepping scheme and the midpoint rule used in the staggered velocity-stress formulation are equivalent.

After discretization of the PML the reflection coefficient is not zero anymore, which generates spurious waves reflected back into the main domain for waves reaching the PML layer at grazing incidence. To overcome these problems, one can modify the complex coordinate stretching used classically in the PML by introducing a shifting of the poles and implementing a Butterworth-like filter in the PML (e.g., Kuzuoglu and Mittra, 1996). This has been first developed for Maxwell's equation (e.g., Roden and Gedney, 2000; Bérenger, 2002a,b) and then adapted to the seismic wave equation in the context of unsplit 2D or 3D finite-difference formulations (e.g., Komatitsch and Martin, 2007; Drossaert and Giannopoulos, 2007; Martin, Komatitsch, and Ezziani, 2008) and by Festa and Vilotte (2005) and Festa, Delavaud, and Vilotte (2005) in the context of a 2D split spectral-element method called GFPML (Generalized Frequency dependent PML).

In this article we extend our unsplit formulation to the spectral-element method and illustrate its efficiency at grazing incidence. In the context of variational techniques such as finite or spectral-element methods, the main advantage of this CPML formulation over classical or other optimized formulations lies in the drastic reduction of memory storage and also easier implementation because of the significantly smaller number of arrays to handle. We explain how the memory variables are involved in velocity and stress calculations. We also show based on 2D numerical examples how waves are efficiently damped at grazing incidence and how large-

amplitude interface waves are absorbed. We finally illustrate how the CPML can be stabilized in some anisotropic cases that are intrinsically unstable in the PML before discretization (Bécache, Fauqueux, and Joly, 2003) by introducing a modification of the damping profile in the two directions as suggested by Meza-Fajardo and Papageorgiou (2008).

2 The classical velocity-stress formulation of the PML

Let us recall some results for the PML applied to the differential form of the seismic equation. For the sake of simplicity the isotropic case is treated hereafter and the extension to the anisotropic case can be simply obtained by using a stiffness tensor with more non-zero terms. For more details the reader is referred for instance to Komatitsch and Martin (2007). In some cases stabilization terms need to be added in the case of an anisotropic medium as will be discussed in further sections.

The differential or 'strong' form of the seismic wave equation can be written as:

$$\rho\, \partial_t^2 \mathbf{u} \;=\; \nabla \cdot \sigma \tag{1}$$

where $\mathbf{u}$ is the displacement vector and $\mathbf{c}$ is the stiffness tensor of the elastic medium. Hooke's law is written as:

$$\begin{aligned} \sigma_{ij} = (\mathbf{c} : \varepsilon)_{ij} &= \lambda\, \delta_{ij} \varepsilon_{kk} + 2\mu\, \varepsilon_{ij} \\ \varepsilon_{ij} &= \frac{1}{2}\left(\frac{\partial u_i}{\partial x_j} + \frac{\partial u_j}{\partial x_i} \right) \end{aligned} \tag{2}$$

where indices i and j can be 1 or 2 in 2D, with the convention of implicit summation over a repeated index, and where δ_{ij} is the Kronecker delta symbol. σ and ε are respectively the stress and strain tensors of the elastic solid, ρ is the density, λ and μ are the Lamé coefficients of the isotropic medium. The frequency-domain form of this equation is

$$-\omega^2 (\rho\, \mathbf{u}) \;=\; \nabla \cdot (\mathbf{c} : \nabla \mathbf{u}) \tag{3}$$

where $\omega = 2\pi f$ denotes angular frequency and where for simplicity we have used the same notation for the fields in the time and frequency domains. In the classical first-order velocity-stress formulation, one first rewrites Eqs. (1) and (2) as :

$$\begin{aligned} \rho \partial_t \mathbf{v} &= \nabla \cdot \sigma \\ \partial_t \sigma &= \mathbf{c} : \nabla \mathbf{v} \end{aligned} \tag{4}$$

where **v** is the velocity vector. The system can also be written using velocity or stress components:

$$\begin{aligned} \rho\,\partial_t v_i &= \partial_j \sigma_{ij} \\ \partial_t \varepsilon_{ij} &= \frac{1}{2}(\partial_j v_i + \partial_i v_j) \\ \sigma_{ij} &= \lambda\,\delta_{ij}\varepsilon_{kk} + 2\mu\,\varepsilon_{ij} \end{aligned} \tag{5}$$

In the frequency domain one then gets:

$$\begin{aligned} \mathrm{i}\omega\rho v_x &= \partial_x \sigma_{xx} + \partial_y \sigma_{xy} \\ \mathrm{i}\omega\rho v_y &= \partial_x \sigma_{xy} + \partial_y \sigma_{yy} \\ \mathrm{i}\omega\sigma_{xx} &= \lambda\,\partial_x v_x + (\lambda+2\mu)\partial_y v_y \\ \mathrm{i}\omega\sigma_{yy} &= (\lambda+2\mu)\partial_x v_x + \lambda\,\partial_y v_y \\ \mathrm{i}\omega\sigma_{xy} &= \mu(\partial_x v_x + \partial_y v_y) \end{aligned} \tag{6}$$

3 The strong velocity-stress formulation of the classical split PML

The main idea behind the PML technique consists in reformulating the derivatives in directions x and y (in 2D) in the PML layers surrounding the physical domain. A damping profile $d_x(x)$ is defined in the PML region such that $d_x = 0$ inside the main domain and $d_x > 0$ in the PML, and a new complex coordinate $\tilde{x}$ is expressed as:

$$\tilde{x}(x) = x - \frac{\mathrm{i}}{\omega}\int_0^x d_x(s)\,\mathrm{d}s. \tag{7}$$

In direction y, a similar damping profile $d_y(y)$ is defined and a new complex coordinate $\tilde{y}$ is expressed as:

$$\tilde{y}(y) = y - \frac{\mathrm{i}}{\omega}\int_0^y d_y(s)\,\mathrm{d}s. \tag{8}$$

Using the fact that

$$\partial_{\tilde{x}} = \frac{\mathrm{i}\omega}{\mathrm{i}\omega + d_x}\partial_x = \frac{1}{s_x}\partial_x, \tag{9}$$

with

$$s_x = \frac{\mathrm{i}\omega + d_x}{\mathrm{i}\omega} = 1 + \frac{d_x}{\mathrm{i}\omega}, \tag{10}$$

and deriving similar expressions of $\partial_{\tilde{y}}$ and s_y, one replaces all x derivatives ∂_x with $\tilde{x}$ derivatives $\partial_{\tilde{x}}$ and y derivatives ∂_y with $\tilde{y}$ derivatives $\partial_{\tilde{y}}$. Equation (6) then becomes:

$$\begin{aligned}
\mathrm{i}\omega\rho v_x &= \partial_{\tilde{x}}\sigma_{xx} + \partial_{\tilde{y}}\sigma_{xy} \\
\mathrm{i}\omega\rho v_y &= \partial_{\tilde{x}}\sigma_{xy} + \partial_{\tilde{y}}\sigma_{yy} \\
\mathrm{i}\omega\sigma_{xy} &= \mu\,(\partial_{\tilde{y}}v_x + \partial_{\tilde{x}}v_y) \\
\mathrm{i}\omega\sigma_{xx} &= (\lambda+2\mu)\partial_{\tilde{x}}v_y + \lambda\,\partial_{\tilde{y}}v_y \\
\mathrm{i}\omega\sigma_{yy} &= \lambda\,\partial_{\tilde{x}}v_x + (\lambda+2\mu)\partial_{\tilde{y}}v_y
\end{aligned} \tag{11}$$

One then uses the mapping (9) to rewrite equation (11) in terms of x rather than $\tilde{x}$ and y rather than $\tilde{y}$. Splitting the equations into two components and using an inverse Fourier transform one goes back to the time domain and obtains the final classical split PML formulation of the isotropic elastic wave equation:

$$\begin{aligned}
(\partial_t + d_x)\rho v_x^1 &= \partial_x\sigma_{xx} \\
(\partial_t + d_y)\rho v_x^2 &= \partial_y\sigma_{xy} \\
(\partial_t + d_x)\rho v_y^1 &= \partial_x\sigma_{xy} \\
(\partial_t + d_y)\rho v_y^2 &= \partial_y\sigma_{yy} \\
(\partial_t + d_x)\sigma_{xy}^1 &= \mu\,\partial_x v_y \\
(\partial_t + d_y)\sigma_{xy}^2 &= \mu\,\partial_x v_y \\
(\partial_t + d_x)\sigma_{xx}^1 &= (\lambda+2\mu)\partial_x v_x \\
(\partial_t + d_y)\sigma_{xx}^2 &= \lambda\,\partial_y v_y \\
(\partial_t + d_x)\sigma_{yy}^1 &= \lambda\,\partial_x v_x \\
(\partial_t + d_y)\sigma_{yy}^2 &= (\lambda+2\mu)\partial_y v_x \\
v_x &= v_x^1 + v_x^2 \\
v_y &= v_y^1 + v_y^2 \\
\sigma_{ij} &= \sigma_{ij}^1 + \sigma_{ij}^2
\end{aligned} \tag{12}$$

Unfortunately, as shown for instance in Komatitsch and Martin (2007) this classical PML formulation does not give satisfactory results at grazing incidence. This can be circumvented via the use of the CPML technique, as presented in the next section.

4 The unsplit variational CPML technique improved at grazing incidence

4.1 Strong velocity-stress formulation of CPML

The CPML technique introduced for Maxwell's equations by Roden and Gedney (2000) and developed for the strong unsplit first-order formulation of the elastic wave equation in Komatitsch and Martin (2007) consists in finding a better choice of the stretching function s_x than that of Eq. (9) by introducing real variables $\alpha_x \geq 0$ and $\kappa_x \geq 1$ such that :

$$s_x = \kappa_x + \frac{d_x}{\alpha_x + \mathrm{i}\omega}. \tag{13}$$

By sake of simplicity we take here $\kappa_x = 1$ because such a choice is satisfactory for many seismic wave propagation problems (e.g., Komatitsch and Martin, 2007). If we denote by $\bar{s}_x(t)$ the inverse Fourier transform of $\frac{1}{s_x}$ then ∂_x can be expressed as:

$$\partial_{\tilde{x}} = \bar{s}_x(t) * \partial_x. \tag{14}$$

After calculating the expression of $\bar{s}_x(t)$ and some algebraic operations we define

$$\zeta_x(t) = -d_x H(t)\, e^{-(d_x+\alpha_x)t}, \tag{15}$$

where H is the Heaviside distribution, and obtain:

$$\partial_{\tilde{x}} = \partial_x + \zeta_x(t) * \partial_x. \tag{16}$$

Since we have null initial conditions, we can approximate the convolution term at time step n following the recursive convolution method of Luebbers and Hunsberger (1992) by:

$$\psi^n \simeq (\zeta_x * \partial_x)^n \simeq \sum_{m=0}^{N-1} Z_x(m)\, (\partial_x)^{n-m} \tag{17}$$

with:

$$\begin{aligned} Z_x(m) &= \int_{m\Delta t}^{(m+1)\Delta t} \zeta_x(\tau)\, \mathrm{d}\tau \\ &= -d_x \int_{m\Delta t}^{(m+1)\Delta t} e^{-(d_x+\alpha_x)\tau}\, \mathrm{d}\tau \\ &= a_x e^{-(d_x+\alpha_x)m\Delta t}. \end{aligned} \tag{18}$$

Setting

$$b_x = e^{-(d_x+\alpha_x)\Delta t} \qquad \text{and} \qquad a_x = \frac{d_x}{d_x+\alpha_x}(b_x-1) \tag{19}$$

the convolution term ψ_x acts as a memory variable on a function f (either a velocity or stress) updated at each time step n as:

$$\psi_x^n(f) = b_x \psi_x^{n-1}(f) + a_x \left(\partial_x f\right)^{n-1/2}, \tag{20}$$

which means that the unsplit CPML formulation can easily be implemented in an existing finite-difference code without PML by simply replacing the spatial derivatives ∂_x with $\partial_x + \psi_x$ and advancing ψ_x in time using the same time evolution scheme as for the other (existing) variables.

4.2 Variational formulation of the elastic equation written in displacement

Following Komatitsch and Tromp (1999), let us recall the variational form of the seismic wave equation. We seek to determine the displacement field produced by a seismic source in a finite Earth model with volume Ω. The boundaries of this volume include a stress-free surface $\partial\Omega$ as well as an absorbing boundary Γ. Seismic waves are reflected by the free surface $\partial\Omega$; ideally, they are completely absorbed by the artificial boundary Γ. The unit outward normal to the boundary $\partial\Omega + \Gamma$ is denoted by $\hat{\mathbf{n}}$. The Earth model may have any number of internal discontinuities; the unit upward normal to such discontinuities is also denoted by $\hat{\mathbf{n}}$. Locations within the model are denoted by the position vector $\mathbf{x} = (x, y)$. For brevity, a component of the position vector will sometimes be denoted using index notation: x_i, $i = 1, 2$, where $x_1 = x$ and $x_2 = y$. Unit vectors in the directions of increasing x_i are denoted by $\hat{\mathbf{x}}_i$, and partial derivatives with respect to x_i are denoted by ∂_i.

In the weak formulation, one uses an integral form, which is obtained by dotting the momentum equation (1) with an arbitrary vector $\mathbf{w}$ and integrating by parts over the model volume Ω, which gives

$$\int_\Omega \rho\, \mathbf{w} \cdot \partial_t^2 \mathbf{u}\, \mathrm{d}\Omega \quad = \quad -\int_\Omega \nabla \mathbf{w} : \sigma\, \mathrm{d}\Omega + \int_\Gamma (\sigma \cdot \hat{\mathbf{n}}) \cdot \mathbf{w}\, \mathrm{d}\Omega. \tag{21}$$

Mathematically, the strong and the weak formulations are equivalent because (21) holds for *any* test vector $\mathbf{w}$. The last integral (on Γ) vanishes because of the free surface condition $\tau = \sigma \cdot \mathbf{n} = \mathbf{0}$.

4.3 Time and space discretization of the classical displacement formulation

To discretize the variational problem we use a spectral-element method (SEM) that has been developed for elastodynamics (e.g., Komatitsch and Vilotte, 1998; Komatitsch and Tromp, 1999). In a SEM the model is subdivided in terms of a number of quadrangle (2D) or hexahedral (3D) elements. In each individual element, functions are sampled at Gauss-Lobatto-Legendre points of integration. The weak formulation (21) is therefore solved on a mesh of quadrangular elements in 2D, which honors both the free surface of the whole medium and its main internal discontinuities and heterogeneities (for instance its fractures or faults).

The unknown wave field is expressed in terms of high-degree Lagrange interpolator polynomials at Gauss-Lobatto-Legendre interpolation points, which results in an exactly diagonal mass matrix that leads to a simple time integration scheme (e.g. Komatitsch et al., 2005). The mass matrix involves the density distribution ρ which may vary from one grid point to another so that fully heterogeneous media can be considered.

If $\mathbf{u}$ contains the displacement vector at all the grid points in the whole mesh then the variational formulation may be rewritten in matrix form as :

$$\mathbf{M}\ddot{\mathbf{u}} + \mathbf{K}\mathbf{u} = \mathbf{F}, \tag{22}$$

where $\mathbf{M}$ denotes the diagonal global mass matrix, $\mathbf{K}$ the global stiffness matrix, and $\mathbf{F}$ the known source term. For detailed expression of these matrices, the reader is referred for instance to Komatitsch and Tromp (1999).

When no PML conditions are used, time discretization of the second-order ordinary differential equation (22) is achieved based upon the following explicit Newmark central finite-difference scheme (e.g., Hughes, 1987) which is second order accurate and conditionally stable, moving the stiffness term to the right-hand side :

$$M\ddot{\mathbf{u}}^{n+1} + K\mathbf{u}^{n+1} = \mathbf{F}^{n+1} \tag{23}$$

where

$$\mathbf{u}^{n+1} = \mathbf{u}^n + \Delta t\dot{\mathbf{u}}^n + \frac{\Delta t^2}{2}\ddot{\mathbf{u}}^n \tag{24}$$

and

$$\dot{\mathbf{u}}^{n+1} = \mathbf{v}^{n+1} = \dot{\mathbf{u}}^n + \frac{\Delta t}{2}[\ddot{\mathbf{u}}^n + \ddot{\mathbf{u}}^{n+1}] \tag{25}$$

At the initial time $t = 0$, zero initial conditions are assumed i.e., $\mathbf{u} = \mathbf{0}$ and $\dot{\mathbf{u}} = \mathbf{0}$.

4.4 Coupling between the displacement and velocity-stress formulations : a mixed formulation

Inside the computational domain, we use the displacement formulation and compute the displacement and velocity fields $\mathbf{u}$ and $\mathbf{v}$ at time t^{n+1} and local stresses Σ^L at time $t^{n+1/2}$. Equations (23) to (25) are solved according to

$$\begin{aligned}
(\mathbf{u},\mathbf{v})^n &\rightarrow \Sigma^{Ln+1/2}(\mathbf{u}^n) = K^L\mathbf{u}^n \\
\Sigma^{Ln+1/2}(\mathbf{u}^n) &\rightarrow \dot{\mathbf{v}}^{n+1} = \mathbf{M}^{-1}K^G\Sigma^{Ln+1/2} \\
(\mathbf{u}^n,\mathbf{v}^n,\dot{\mathbf{v}}^{n+1}) &\rightarrow (\mathbf{u},\mathbf{v})^{n+1}
\end{aligned} \tag{26}$$

where $\mathbf{M}$ is the diagonal global mass matrix, $\Sigma^{Ln+1/2}$ is the local stress tensor in each element, $K^G\Sigma^{Ln+1/2}$ is the global stress tensor calculated by assembling the local stiffness matrices K^L at the common edges shared by the elements (all calculated at time $t^{n+1/2}$), and K^G is the operator that assembles all the internal force contributions at each global node of the mesh including those located at the edges common to different spectral elements.

Following Festa and Vilotte (2005), inside the PML we use a velocity-stress formulation of the spectral-element method and a second-order staggered temporal integration introduced in some finite-difference and finite-element methods (e.g., Virieux, 1986; Cohen and Fauqueux, 2005; Festa and Vilotte, 2005) which is equivalent to the second-order Newmark time scheme:

$$\begin{aligned}
(\mathbf{u},\mathbf{v})^n &\rightarrow \dot{\Sigma}^{Ln+1/2}(\mathbf{v}^n) = K^L\mathbf{v}^n \\
\dot{\Sigma}^{Ln+1/2}(\mathbf{v}^n) &\rightarrow \Sigma^{Ln+1/2}(\mathbf{v}^n) \\
\Sigma^{Ln+1/2}(\mathbf{v}^n) &\rightarrow \dot{\mathbf{v}}^{n+1} = \mathbf{M}^{-1}K^G\Sigma^{Ln+1/2} \\
(\mathbf{u}^n,\mathbf{v}^n,\dot{\mathbf{v}}^{n+1}) &\rightarrow (\mathbf{u},\mathbf{v})^{n+1}
\end{aligned} \tag{27}$$

where $\dot{\Sigma}^{Ln+1/2}(\mathbf{v}^n)$ is the first derivative in time of the local stress tensor. The assembling operator of all force contributions at the global points or edges shared by different elements is denoted by K^G, as in the displacement formulation. As memory variables are exactly zero on both sides of the interface between the PML and the inner computational domain and as the stresses are calculated on both sides based on the hybrid procedure described above, the assembly of the stiffness matrices is performed naturally and the five variables v_x, v_y, σ_{xx}, σ_{yy}, σ_{xy} can be calculated in the inner domain and at the base of the PML. Let us now see how these variables as well as the memory variables are computed in the PML using the variational velocity-stress formulation.

4.5 Integration of CPML using a velocity-stress formulation

Restricting ourselves to the case of flat PML layers parallel to the coordinate axes x and y, and defining damping memory variables Ψ that are functions of velocities and stresses derivatives, we can rewrite the weak formulation of the velocity-stress equations as:

$$\begin{aligned}
\int_\Omega \rho\, w_x \cdot \partial_t v_x \,\mathrm{d}\Omega &= -\int_\Omega (\sigma_{xx}\partial_x w_x + \sigma_{xy}\partial_y\ w_x)\,\mathrm{d}\Omega \\
&+ \int_\Omega (\Psi(\partial_x \sigma_{xx}) + \Psi(\partial_y \sigma_{xy}))\, w_x \mathrm{d}\Omega \\
&+ \int_\Gamma (\sigma_{xx} n_x + \sigma_{xy} n_y) w_x \mathrm{d}\mathbf{x}, \\
\int_\Omega \rho\, w_y \cdot \partial_t v_y \,\mathrm{d}\Omega &= -\int_\Omega (\sigma_{xy}\partial_x w_y + \sigma_{yy}\partial_y w_y)\,\mathrm{d}\Omega \\
&+ \int_\Omega (\Psi(\partial_x \sigma_{xy}) + \Psi(\partial_y \sigma_{yy}))\, w_y \mathrm{d}\Omega \\
&+ \int_\Gamma (\sigma_{xy} n_x + \sigma_{yy} n_y)\, w_y \mathrm{d}\mathbf{x}, \\
\int_\Omega \partial_t \sigma_{xx}\, \tau_{xx}\,\mathrm{d}\Omega &= \int_\Omega ((\lambda + 2\mu)\partial_x v_x + 2\mu\partial_y v_y)\, \tau_{xx}\,\mathrm{d}\Omega \\
&+ \int_\Omega ((\lambda + 2\mu)\Psi(\partial_x v_x) + 2\mu\Psi(\partial_y v_y))\, \tau_{xx}\mathrm{d}\Omega \\
\int_\Omega \partial_t \sigma_{xy}\, \tau_{xy}\,\mathrm{d}\Omega &= \int_\Omega \mu(\partial_y v_x + \partial_x v_y)\, \tau_{xy}\,\mathrm{d}\Omega \\
&+ \int_\Omega \mu(\Psi(\partial_y v_x) + \Psi(\partial_x v_y))\, \tau_{xy}\mathrm{d}\Omega, \\
\int_\Omega \partial_t \sigma_{yy}\, \tau_{yy}\,\mathrm{d}\Omega &= \int_\Omega (\lambda\partial_x v_x + (\lambda + 2\mu)\partial_y v_y)\, \tau_{yy}\,\mathrm{d}\Omega \\
&+ \int_\Omega (\lambda\Psi(\partial_x v_x) + (\lambda + 2\mu)\Psi(\partial_y v_y))\, \tau_{yy}\mathrm{d}\Omega
\end{aligned} \tag{28}$$

After some algebraic manipulation and taking into account the fact that $\mathbf{v} = (v_x, v_y)$ and $\sigma = (\sigma_{xx}, \sigma_{yy}, \sigma_{xy})$ belong respectively to $H^1(\Omega)\times H^1(\Omega)$and $L^2(\Omega)\times L^2(\Omega)\times L^2(\Omega)$, the memory variables Ψ are calculated in a weak and tensorial form as fol-

lows:

$$
\begin{aligned}
(\int_\Omega \Psi(\partial_i v_j)\,\tau_{ij}\mathrm{d}\Omega)^{n+1} &= (\int_\Omega b(x_i)\Psi(\partial_i v_j)\,\tau_{ij}\mathrm{d}\Omega)^n + (\int_\Omega a(x_i)\partial_i v_j\,\tau_{ij}\mathrm{d}\Omega)^{n+1/2} \\
(\int_\Omega \Psi(\partial_i \sigma_{ij})\,w_i\mathrm{d}\Omega)^{n+1} &= (\int_\Omega b(x_i)\Psi(\partial_i \sigma_{ij})\,w_i\mathrm{d}\Omega)^n - (\int_\Omega \sigma_{ij}\,\partial_i(a(x_i)w_i)\mathrm{d}\Omega)^{n+1/2} \\
&+ (\int_\Gamma a(x_i)\sigma_{ij}n_i\Psi(\partial_i\sigma_{ij})\,w_i\mathrm{d}\Gamma)^{n+1/2}
\end{aligned}
\tag{29}
$$

Equations (28) and (29), which correspond to computations in the PML, can be summarized in the following time integration scheme:

$$
\begin{aligned}
[\mathbf{u},\mathbf{v},\Psi(\mathbf{v})]^n &\rightarrow \dot{\Sigma}^{Ln+1/2}(\mathbf{v}^n) = K^L\mathbf{v}^n \\
&\quad + K_v^L\Psi^L(\mathbf{v}^n) \\
\dot{\Sigma}^{Ln+1/2}(\mathbf{v}^n) &\rightarrow \Sigma^{Ln+1/2}(\mathbf{v}^n) \\
\Sigma^{Ln+1/2}(\mathbf{v}^n) &\rightarrow \Psi(\Sigma^{Ln+1/2}) \\
\left[\Psi(\Sigma^{Ln+1/2}),\Sigma^{Ln+1/2}\right] &\rightarrow \dot{\mathbf{v}}^{n+1} = \mathbf{M}^{-1}(K^G\Sigma^{Ln+1/2} + K_s^G\Psi(\Sigma^{Ln+1/2})) \\
(\mathbf{u}^n,\mathbf{v}^n,\dot{\mathbf{v}}^{n+1}) &\rightarrow [\mathbf{u},\mathbf{v},\Psi(\mathbf{v})]^{n+1}
\end{aligned}
\tag{30}
$$

where K_v^L denotes a diagonal mass matrix for the integration of the memory variables related to velocity components that is similar to the mass matrix M, and K_s^G is the global assembling operator of the memory variables related to the stress variables. We have $\Psi = 0$ at the interface between the inner and CPML domains. Finally, the system of equations in the inner domain plus the PML layers is solved based on Equations (26) to (30).

In the corners of the PML (i.e., the areas of the grid that belong to both the vertical and horizontal layers), the 2D model consists of 13 equations: 2 equations for the velocity vector, 3 for the stress tensor, and 8 for memory variables. This is a significant improvement in terms of memory storage over the 20 equations necessary when the classical PML or the optimized split PML (e.g., Festa and Vilotte, 2005) is used.

Let us mention that we could formulate the time evolution equations of auxiliary memory variables as differential equations rather than formulating them as convolutional terms as shown by Gedney and Zhao (2009) who introduce an alternate second-order accurate update formulation in time based on a finite-difference approximation with comparable accuracy. An advantage of this formulation lies in the fact that if a higher-order time integration for the SEM were used, for instance a symplectic scheme (Simo, Tarnow, and Wong, 1992; Nissen-Meyer, Fournier, and

Dahlen, 2008), one could apply it and equation (28) would not change. The only change would be that the time-update of the auxiliary term ψ would be based on an ordinary differential equation rather than a recursive convolutional form. In this way, a higher order time advancement scheme can be implemented more easily.

5 Numerical tests

5.1 Case of a thin isotropic homogeneous slice

In order to study the efficiency of the CPML at grazing incidence, we consider a first experiment in which we simulate the propagation of waves in a 2D homogeneous elastic isotropic medium of size 5000 m $\times$ 1250 m surrounded by four PML layers of 13 grid points (i.e., three spectral elements) each. The pressure and shear wave velocities are $V_p = 3000$ m/s and $V_s = 2000$ m/s and density $\rho = 2000$ kg/m^3. In each spectral element we use a polynomial degree $N = 4$ and the number of Gauss-Lobatto-Legendre collocation points is therefore $(N+1)^2 = 25$. The grid (including the PML layers) has a total size of (160$\times N$+1) $\times$(40$\times N$+1)= 103,201 points.

We select a time step $\Delta t = 2$ ms, i.e., a Courant-Friedrichs-Lewy (CFL) stability value of 0.56. The simulation is performed for 50,000 time steps, i.e., for a total duration of 100 s. A vertical point source is located close to the top PML layer at 9 grid points from its base in ($x_s = 4000$ m, $y_s = 1062.5$ m). A pressure (P) wave and a slower shear (S) wave are therefore generated with a polarization of the S wave orthogonal to the bottom PML layer, which allows us to test the efficiency of the CPML at grazing incidence. The source time function is the second derivative of a Gaussian with a dominant frequency $f_0 = 14$ Hz, shifted in time by $t_0 = 0.085$ s in order to have quasi-null initial conditions.

Following for instance Gedney (1998) and Collino and Tsogka (2001), the damping profile in the PML is chosen as $d_x(x) = d_0 \left(\frac{x}{L}\right)^N$ along the x axis and $d_y(y) = d_0 \left(\frac{y}{L}\right)^N$ along the y axis, where L is the thickness of the absorbing layer, $N = 2$ and $d_0 = -\frac{(N+1)V_{pmax}\log(R_c)}{2L} \simeq 217.6$, V_{pmax} being equal to the speed of the pressure wave and R_c being the target theoretical reflection coefficient, chosen here as 0.1 %. As in Roden and Gedney (2000), we make α_x and α_y vary in the PML layer between a maximum value $\alpha_{\max}$ at the beginning of the PML and zero at the top. These functions are defined as $\alpha_{\max}[1-(x/L)^m]$ where m will take values 1, 2 or 3 to study its influence when simulations are performed for a long period of time. We also take $\alpha_{\max} = 0$ or $\alpha_{\max} = \pi f_0$, where f_0 is the dominant frequency of the source defined above, in order to study the influence of that parameter on the solution. On the external edges of the grid, i.e., at the top of each PML, we impose a Dirichlet condition for the velocity vector ($\mathbf{v} = \mathbf{0}$ for all t). Because of the aspect ratio of

the grid and the location of the source close to the right PML, the waves reach the PML layers at grazing incidence in several areas of the mesh.

Snapshots at different times (Figure 1) do not exhibit significant spurious oscillations in the case of the CPML condition with $\alpha_{\max} = \pi f_0$. The pressure wave and the shear wave are gradually absorbed in the PMLs. On the contrary, in the case of a non shifted CPML (i.e., $\alpha_{\max} = 0$), which is very similar to the classical PML but not strictly equivalent because the discrete convolution in equation (17) is evaluated based on an approximation in the CPML technique, spurious modes appear along the PML, as can be observed in the snapshots of Figure 2. This spurious energy is generated along the bottom PML by waves traveling at grazing incidence.

Let us record the vertical component of the displacement vector at two receivers located close to the edges of the grid, on the left and on the right of the slice in the top corners, 9 grid points below the lower PML in ($x_1 = 300$ m, $y_1 = 1062.5$ m) and ($x_2 = 4700$ m, $y_2 = 1062.5$ m). In Figure 3, solutions with CPML and non shifted CPML are compared with a reference solution computed with the SEM used on a much larger computational domain. The difference is small in the case of CPML while the solution computed with the non shifted CPML is significantly distorted.

Let us now study the decay of energy in the mesh in order to analyze more precisely the efficiency of the CPML at grazing incidence. We represent in Figure 4a the decay in time of total energy E:

$$E = \frac{1}{2}\rho \|\mathbf{v}\|^2 + \frac{1}{2}\sum_{i=1}^{D}\sum_{j=1}^{D}\sigma_{ij}\varepsilon_{ij} \tag{31}$$

over 5 seconds in the inner part of the model (i.e., in the medium without the four PML layers) for the simulation presented in Figure 1. Between approximately 0 s and 0.17 s the source injects energy into the system and then the energy carried by the P and S waves is gradually absorbed by the PML layers, and after approximately 3 s both waves should have disappeared and there should remain no energy in the medium. All the remaining energy is therefore spurious. Let us note that total energy decays very quickly by approximately 7 to 8 orders of magnitude between 3 s and 10 s.

It is also interesting to study the issue of the stability of the CPML for long times. It is known that in numerous PML models, for instance in the case of Maxwell's equations, weak or strong instabilities can develop for long simulations (e.g., Abarbanel, Gottlieb, and Hesthaven, 2002; Bécache and Joly, 2002). To analyze long-time stability from a numerical point of view, we show in Figure 4b the evolution of total energy over 100 s (i.e., 50,000 time steps). It decreases continuously until reaching a value of about 10^{-9} J and no instabilities are observed on this semi-logarithmic scale, which means that the discrete CPML is stable up to 50,000 steps. In the case

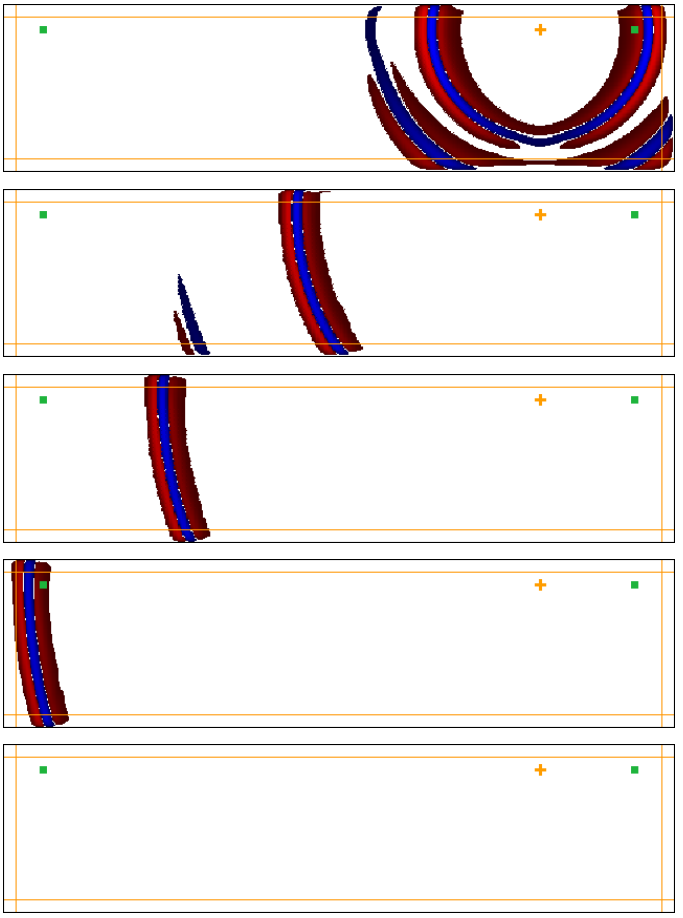

Figure 1: Snapshots at time 0.5 s, 1 s, 1.5 s, 2 s and 2.5 s of the propagation of P-SV waves generated by a second derivative of a Gaussian time wavelet source located in a homogeneous elastic slice at the orange cross in ($x = 4000$ m, $y = 1062.5$ m) under the upper PML layer. CPML layers with a frequency shift are implemented in the four edges represented by the four orange lines. No significant spurious reflections are observed, even at grazing incidence, which shows the efficiency of the variational formulation of the unsplit CPML.

of the non shifted CPML the decay of energy is not continuous due to the spurious energy that is sent back into the medium, as we have seen in Figure 2. This occurs until total energy reaches a final value very similar to that obtained in the case of the shifted CPML when all the spurious waves have been absorbed in turn and almost no spurious energy remains in the mesh.

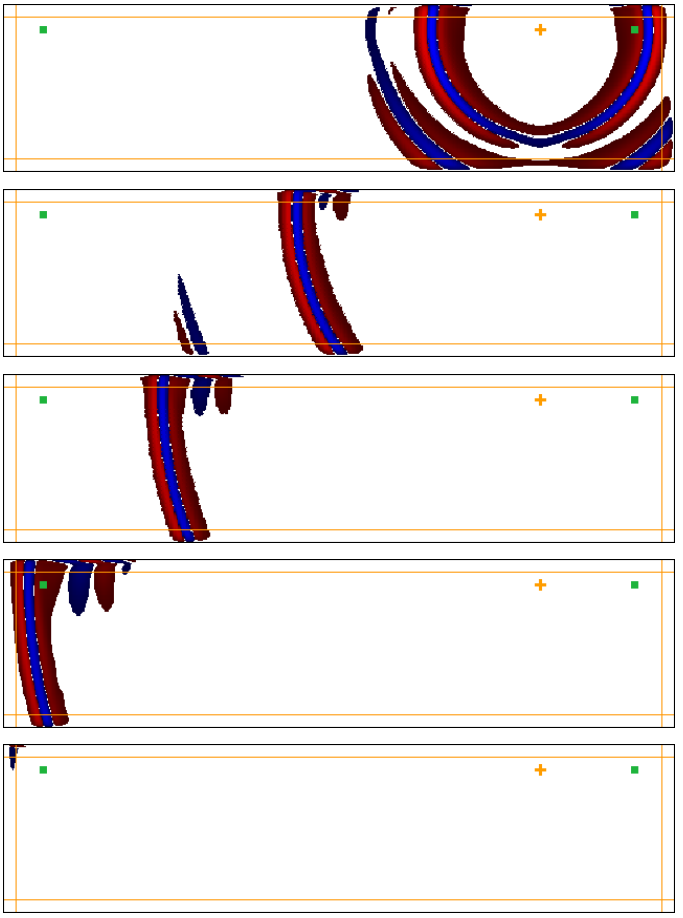

Figure 2: Same as in Figure 1 but for a CPML with no frequency shift. Significant spurious reflections traveling along the PML and coming back into the main domain can be observed at grazing incidence.

5.2 Isotropic heterogeneous case with topography

We now study a two-layer medium with topography in order to illustrate how CPML absorbs surface waves (i.e., Rayleigh waves here). The topography and the interface between the two layers have a height variation of approximately 200 m (Figure 5). The two layers have pressure and shear velocities of $V_p = 3000$ m/s and $V_s = 2000$ m/s for the top layer and $V_p = 2500$ m/s and $V_s = 1500$ m/s for the bottom layer. Density is 2000 kg/m^3 in the top layer and 1500 kg/m^3 in the bottom layer. The interface is located around $y = 750$ m. A vertical point source force is

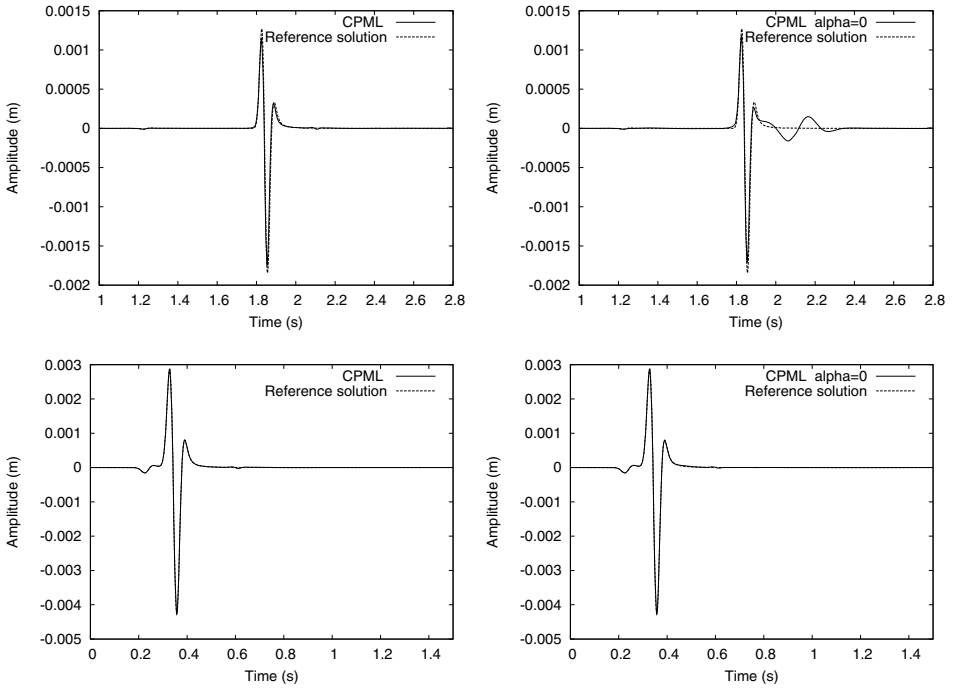

Figure 3: (Left): Time evolution of the numerical solution with shifted CPML (dotted line) in a thin homogeneous elastic slice surrounded by four PMLs for the vertical component of displacement recorded at the first (top) and second (bottom) receiver (represented by green squares in Figure 1) compared to a reference solution computed on a four-times larger grid (dashed line). At these receivers located close to the upper CPML layer (9 grid points away from its beginning) the agreement is good in spite of the grazing incidence and no spurious oscillations are observed. (Right): Spurious oscillations and signal distortion appear when no frequency shift is added because of the generation of spurious waves traveling along the PML at grazing incidence and coming back into the inner domain, as seen in Figure 2. The shear wave is particularly distorted at the first and second receivers.

located at the surface in order to generate two large-amplitude Rayleigh waves and study how they are absorbed. The source has a dominant frequency $f_0 = 8$ Hz and is shifted in time by $t_0 = 0.15$ s. The grid (including the PML layers) has a total size of $140 \times 35 = 4900$ elements (i.e. 79,101 unique grid points) and the time step is 0.4 ms.

Snapshots (Figure 5) for the CPML solution do not exhibit significant spurious oscillations. The Rayleigh wave, the interface waves and all the reflected and con-

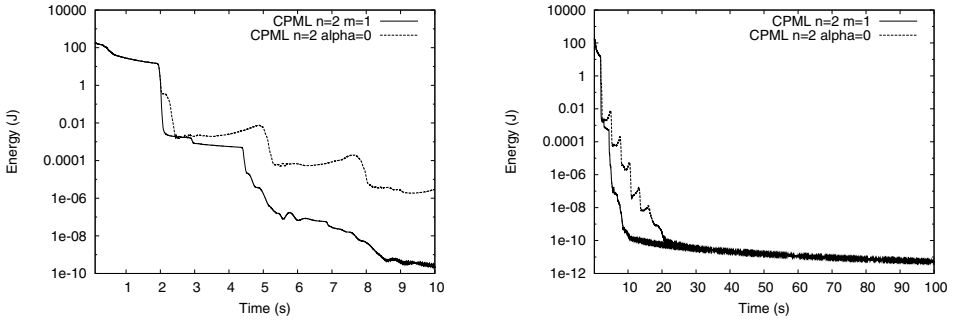

Figure 4: (Left): Decay of total energy in semi-logarithmic scale for the homogeneous elastic medium of Figures 1 and 2 for a medium time period of 10 s of simulation for shifted CPML (solid line) and non shifted CPML (dashed line). In the case of CPML, energy decreases step by step by 6 orders of magnitude for different values of exponent m of α_x and for a quadratic evolution of d_x ($N = 2$). In the case of non shifted CPML, energy decay is less efficient owing to the re-injection of spurious waves from the PML boundaries into the inner domain. (Right): Energy decay for a longer time period (100 s). No instabilities are observed, which means that the discrete CPML is stable up to 50,000 time steps. One can notice tiny oscillations owing to the fact that total energy is so small that we start to see the effect of roundoff of floating-point numbers of the computer.

verted P and S waves are gradually absorbed. On the contrary, in Figure 6 for the case of CPML with no shift of the poles (i.e., $\alpha = 0$ and $\kappa = 1$ in equation (13)), large oscillations appear at grazing incidence around 8 s.

In Figure 7 we compare at the first receiver located in (x_1 = 300 m, y_1 = 1245 m) and at the second receiver located in (x_2 = 4700 m, y_2 = 1235 m) seismograms of the vertical component of the displacement vector computed with CPML with and without shift to a reference solution computed on a much larger computational grid. The CPML solution with shift shows a very good agreement, while large discrepancies can be observed in the case of CPML without shift.

Let us now study the decay of total energy to analyze numerically the stability at long time periods and let us therefore make the simulation last for 40 s (i.e., 100,000 time steps). Figure 8 illustrates that energy decays very quickly by 6 orders of magnitude in 5 s, the time for the large-amplitude Rayleigh waves and all the body waves to be efficiently absorbed. Then, the remaining spurious waves are absorbed in turn, which reduces total energy by 10 orders of magnitude around a time period of about 10 s. For longer time periods up to a total duration of 40 s (i.e., 100,000 time steps) the CPML solution is stable and total energy reaches a value

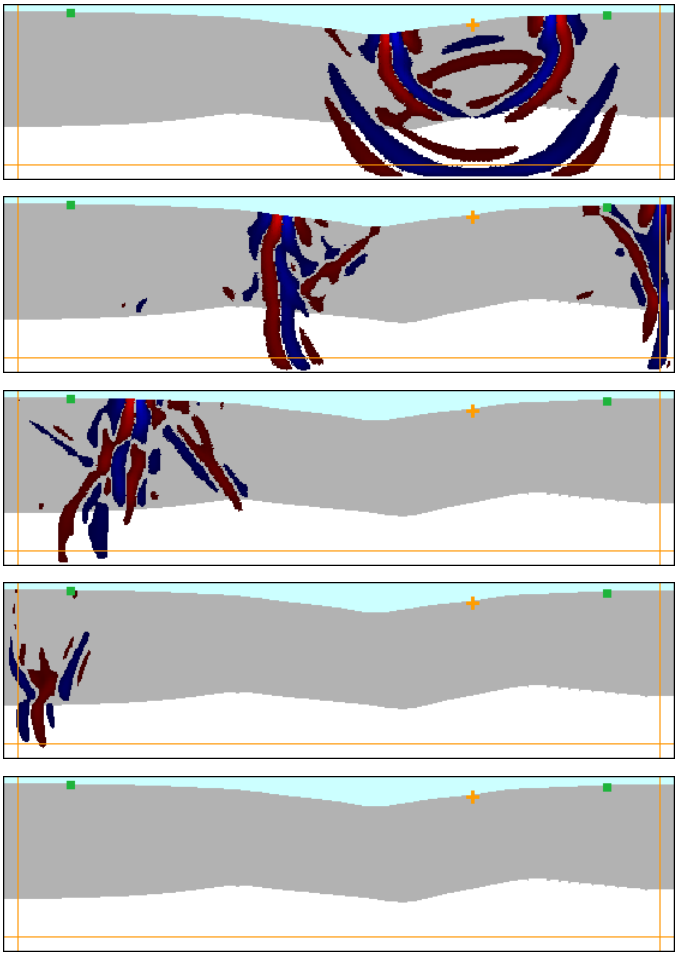

Figure 5: Snapshots at times 0.6 s, 1.2 s, 2 s, 2.8 s and 7.6 s of the propagation of pressure, shear and surface (i.e., Rayleigh) waves as well as transmitted, converted or reflected waves in a two-layer elastic medium excited with a vertical-force wavelet source (second time derivative of a Gaussian) located at $x = 4000$ m exactly on the surface. Shifted CPML layers are implemented on the two vertical edges and at the bottom (orange lines). All body waves as well as the highly energetic Rayleigh wave are efficiently absorbed by the CPML layers. No significant spurious reflections are observed once all waves have been absorbed after approximately 3 s.

of about 10^{-9} J, with tiny oscillations that are due to round-off of the processor for such very small values. On the contrary, in the case of non shifted CPML, total

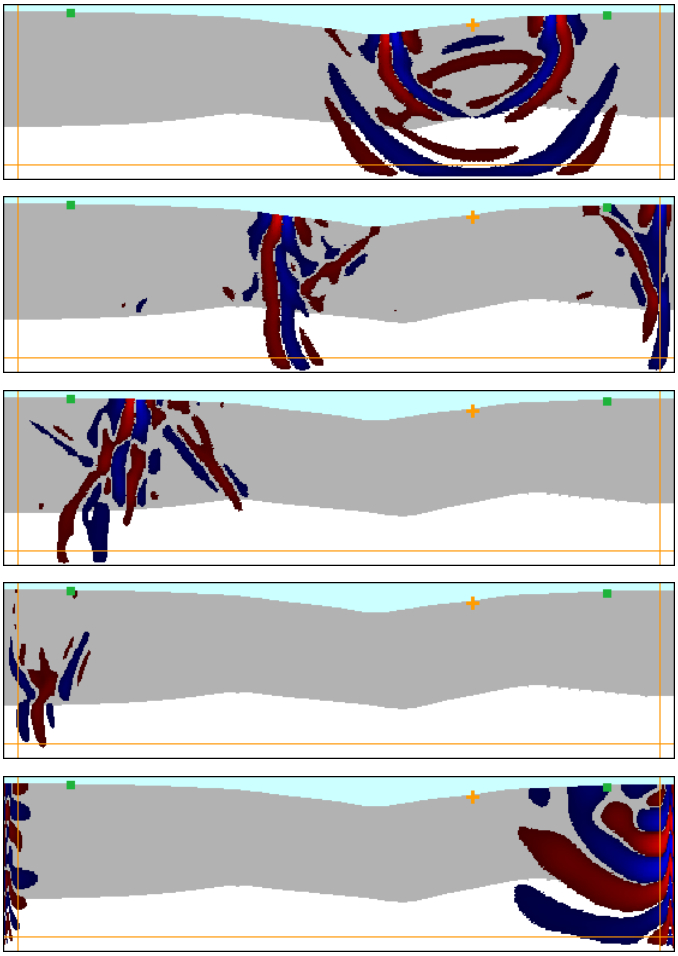

Figure 6: Same as in Figure 5 but with non shifted CPML. After 7 s spurious oscillations reflected off the PML layers can be clearly observed.

energy decreases for 5 s but then starts to grow very quickly due to unstable modes amplifying in the PML and contaminating the inner domain. If we take a linear variation ($m = 1$) of the α_x function instead of taking a degree $m = 2$ or 3, the decay of energy is more pronounced in the first 10 s and then energies reach very similar values for $m = 1, 2, 3$ beyond 10 s. The Rayleigh wave is more difficult to absorb, which explains the fact that the decay is not as steep as in the previous test for a homogeneous medium. Energy is however drastically reduced by more than 10 orders of magnitude.

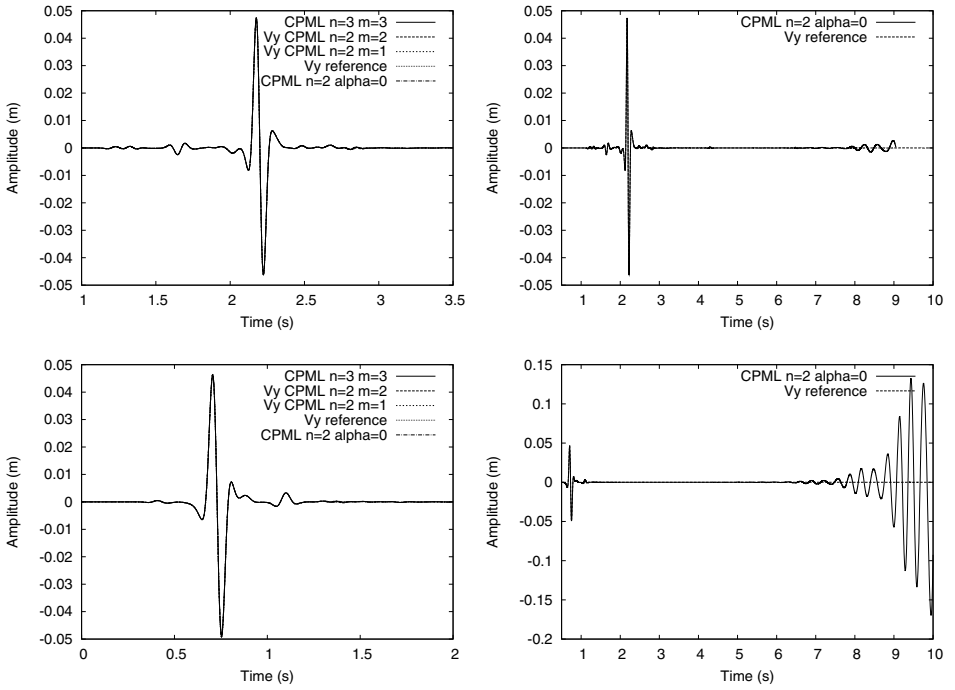

Figure 7: (Left): Time evolution of the numerical solutions with shifted CPML (dotted line) for the model of Figure 5 for the vertical component of displacement recorded at the first receiver (top) located in ($x = 4700$ m, $y = 1245$ m) at the top left of the snapshots (green squares in Figure 5) exactly on the surface and at the second receiver (bottom) located in ($x = 4700$ m, $y = 1235$ m) at the top right exactly on the surface, compared to a reference solution (tiny dashed line) computed on a four-times larger computational grid. The agreement is good in spite of the grazing incidence and no significant spurious oscillations are observed. (Right): Same as the left figures but with no frequency shift in the CPML. Oscillations appear after 8 s because of the generation of spurious waves traveling along the PML at grazing incidence and coming back into the inner domain. These oscillations can evolve into growing instabilities.

5.3 Stabilization of anisotropic media

Coefficients a_x and b_x (i.e., equations (19)) do not depend on the physical properties of the materials. Therefore, the CPML technique can in principle be used also in the case of anisotropic media. Unfortunately some anisotropic materials are intrinsically unstable when the classical PML formulation is introduced, even before

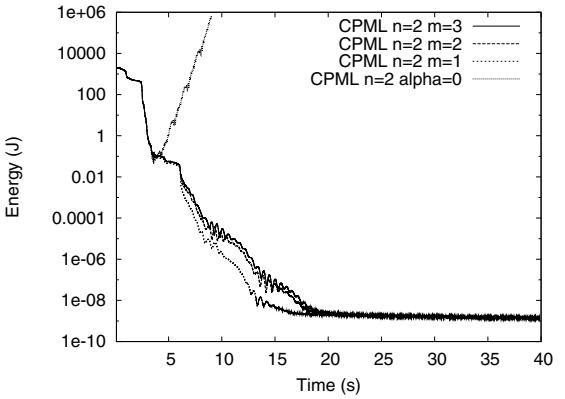

Figure 8: Total energy decay in semi-logarithmic scale for the heterogeneous elastic medium of Figures 5 and 6 for a long time period of 70 s of simulation for shifted CPML and non shifted CPML ($\alpha = 0$). No instabilities are observed when a frequency shift is used, which means that the discrete CPML is stable up to 70,000 time steps. It seems that a linear variation of α_x ($m = 1$) and a quadratic polynomial (N=2) describing d_x are reasonable values and provide better energy decay. All these cases finally lead to similar energies around 10^{-9} J beyond 20 s. After 20 s one can notice tiny oscillations owing to the fact that total energy is so small that we start to see the effect of roundoff of floating-point numbers of the computer. In the case of non shifted CPML (α =0), energy starts to increase very quickly after approximately 5 s owing to growing instabilities that develop in the PML layers.

discretization by a numerical scheme (e.g., Bécache, Fauqueux, and Joly, 2003). But Meza-Fajardo and Papageorgiou (2008) have shown that modifications can be introduced in the damping profiles to stabilize the discrete system. It is possible to introduce corrections in the damping profiles d_x by adding an extra damping profile in the orthogonal direction i.e. writing $d_x(x,y) = d_x^x(x) + d_x^y(y)$, $d_x^x(x)$ being the classical damping profile in the x direction inside the PML (as in the previous sections) and $d_x^y(y) = c_x(x,y)d_x^x(x)$ the corrected damping profile in direction y. $c_x(x,y)$ is generally a function varying between 0 and 1 inside the PML. The same can be done for d_y (see Figure 9). Meza-Fajardo and Papageorgiou (2008) used this correction for the split formulation of the PML conditions in a finite-difference context. Here we introduce it in our unsplit variational CPML technique with no extra cost in terms of memory storage.

Let us use strongly anisotropic materials inside the PML layers: an apatite crystal of stiffness coefficients in reduced Voigt notation $c_{11} = 1.4 \times 10^{11}$ N.m, $c_{22} =$

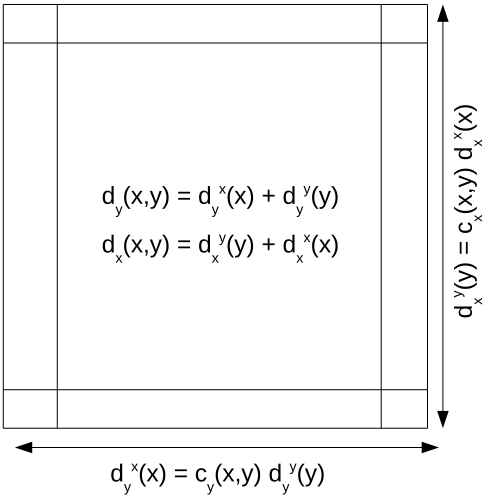

Figure 9: Definition of the corrected damping profiles in all the PML layers of Meza-Fajardo and Papageorgiou (2008) that are used to stabilize the CPML formulation for anisotropic media.

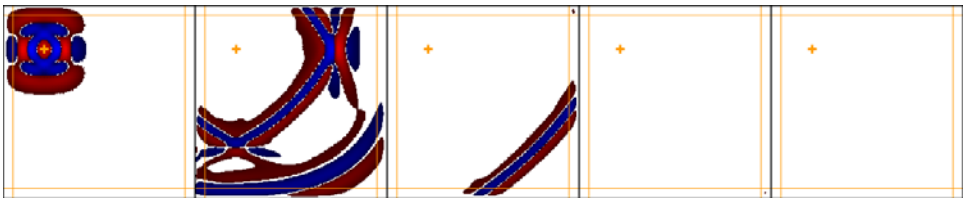

Figure 10: Snapshots at times 20, 60, 100, 140 and 500 μs for an apatite crystal without a frequency shift when a corrected damping profiles are introduced. No instabilities are observed, while the same snapshots without correction shown in Komatitsch and Martin (2007) (Figure 10 of that article) show that the simulation with no correction is unstable. Snapshots for a shifted CPML are very similar and therefore not shown here.

1.67×10^{11} N.m, $c_{12} = 6.6 \times 10^{10}$ N.m, $c_{33} = 6.63 \times 10^{10}$ N.m, and density $\rho =$ 3200 kg/m^3; or a zinc crystal ($c_{11} = 1.65 \times 10^{11}$ N.m, $c_{22} = 6.2 \times 10^{10}$ N.m, $c_{12} = 5 \times 10^{10}$ N.m, $c_{33} = 3.96 \times 10^{10}$ N.m, and density $\rho = 7100$ kg/m^3). As explained by Bécache, Fauqueux, and Joly (2003) and demonstrated numerically in Komatitsch and Martin (2007), these models are intrinsically unstable at high

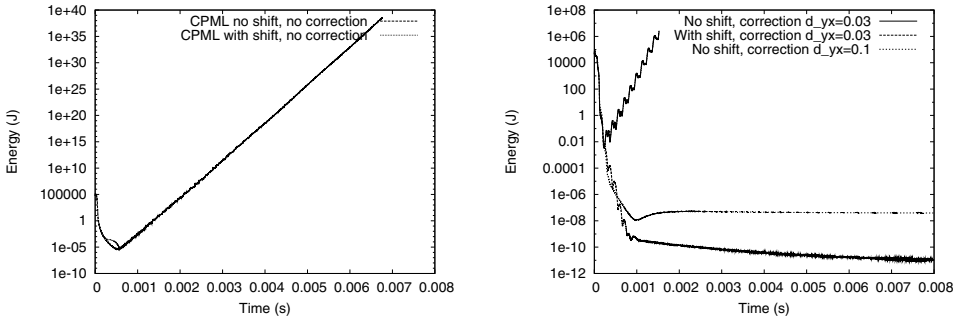

Figure 11: (Left): Decay of total energy for an apatite crystal for CPML with (solid line) and without (dashed line) frequency shift when no correction is implemented. The PML is then unstable at high frequency (Bécache, Fauqueux, and Joly, 2003), i.e., total energy increases. (Right): Instabilities do not appear any more when corrections of the damping profiles are added as suggested by Meza-Fajardo and Papageorgiou (2008).

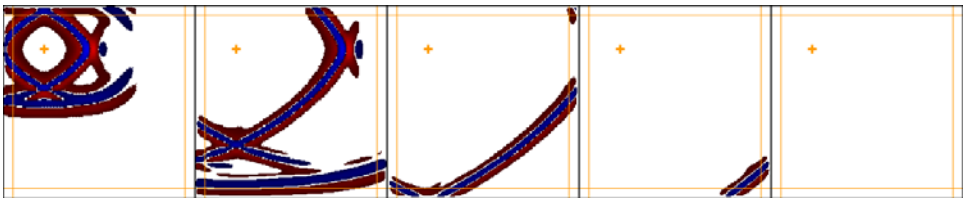

Figure 12: Same as Figure 10 but for a zinc crystal at times 40, 80, 120, 160 and 600 μs.

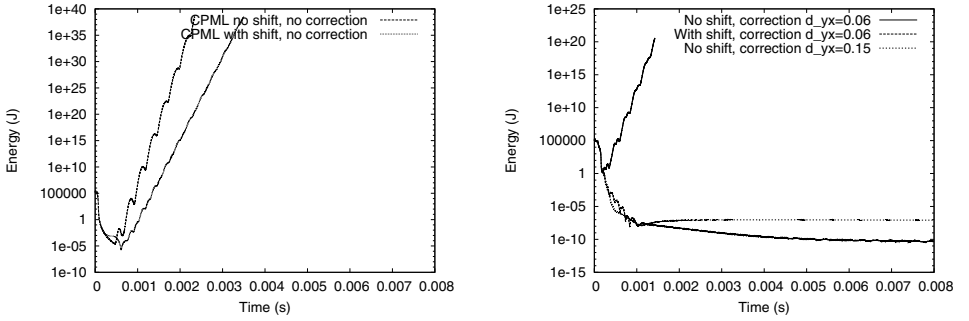

Figure 13: Same as Figure 11 but for a zinc crystal.

frequency because at least one of the following conditions is violated:

$$\begin{aligned}((c_{12}+c_{33})^2-c_{11}(c_{22}-c_{33}))\,((c_{12}+c_{33})^2+c_{33}(c_{22}-c_{33}))\le 0\\ (c_{12}+2c_{33})^2-c_{11}\,c_{22}\le 0\\ (c_{12}+c_{33})^2-c_{11}\,c_{22}-c_{33}^2\le 0\end{aligned} \tag{32}$$

Let us therefore use a source with high frequency content: the second time derivative of a Gaussian with a dominant frequency of 100 Hz. Indeed, in the case of both apatite and zinc crystals, the total energy quickly blows up when no corrections of the damping functions are introduced (Figures 11 and 13). This means that the simulations become unstable at time periods beyond 0.001 s independently of using a frequency shift in CPML or not. However, using the correction of Meza-Fajardo and Papageorgiou (2008) it is possible to enforce the high-frequency stability conditions for the quasi-shear wave of equation (32) by using a suitable value of the correction factor c_x. In Figures 10 (apatite) and 12 (zinc), we show snapshots at different times (short, medium and long time periods) of wave propagation for the two fully anisotropic materials under study when the corrections of damping profiles are introduced. The simulations remain stable for long time periods even for such a source located in a corner of the computational domain and close to the base of the PML, which is a difficult case because a very significant part of the energy of the source is quickly sent into the PML layers. Here, $c_x = c_y = 0.03$ (apatite) or $c_x = c_y = 0.06$ (zinc) allow for a stabilization of CPML when a frequency shift is used, while higher values of 0.1 for apatite and 0.15 for zinc are needed to stabilize it when no frequency shift is used (Figures 11 and 13). Total energy diverges when no correction is used while it decays by around 12 orders of magnitude until reaching values around 10^{-10} J or 10^{-11} J at long time periods of 0.008 s (200,000 time steps) when corrections are used. If high damping corrections are added in the non shifted case, total energy decay is enforced at the expense of a small distortion of the wave patterns near the boundaries (not shown here).

6 Conclusions and future work

We have extended the unsplit convolutional perfectly matched layer (CPML) technique to the variational formulation of the seismic wave equation discretized based upon a spectral-element method. We have been able to absorb not only pressure and shear waves in a homogeneous medium but also surface waves in a heterogeneous medium in the presence of topography. The introduction of corrections in the damping profiles along the different coordinate axes has stabilized the numerical technique at high frequency in the case of anisotropic media that are intrinsically unstable when the classical PML is used. The memory storage of the CPML is

smaller by about 35% compared to the classical split PML (if only split variables v_i^j are stored in memory) or to optimized split PMLs such as the GFPML technique (Festa and Vilotte, 2005), and by about 48% if split variables and total fields v_i are both stored in memory. In 3D the CPML technique reduces the memory storage by about 44% compared to the classical split PML or to the GFPML if only split variables are stored in memory, and by about 53% if split variables and total fields v_i are both stored in memory. In the case of an implementation of the spectral-element method on a parallel computer (e.g., Martin, Komatitsch, Blitz, and Le Goff, 2008), efforts will need to be made in order to balance the number of calculations inside and outside the PML because the number of computations is higher inside the PMLs than outside.

Acknowledgement: The authors thank Julien Diaz for fruitful discussions on the variational formulation.

References

Abarbanel, S.; Gottlieb, D.; Hesthaven, J. S. (2002): Long-time behavior of the perfectly matched layer equations in computational electromagnetics. *J. Sc. Comp.*, vol. 17, pp. 405–422.

Abreu, A. I.; Mansur, W. J.; Soares-Jr, D.; Carrer, J. A. M. (2008): Numerical computation of space derivatives by the complex-variable-differentiation method in the convolution quadrature method based BEM formulation. *CMES: Computer Modeling in Engineering & Sciences*, vol. 30, no. 3, pp. 123–132.

Alterman, Z.; Karal, F. C. (1968): Propagation of elastic waves in layered media by finite difference methods. *Bull. Seismol. Soc. Am.*, vol. 58, pp. 367–398.

Bao, H.; Bielak, J.; Ghattas, O.; Kallivokas, L. F.; O'Hallaron, D. R.; Shewchuk, J. R.; Xu, J. (1998): Large-scale simulation of elastic wave propagation in heterogeneous media on parallel computers. *Comput. Methods Appl. Mech. Engrg.*, vol. 152, pp. 85–102.

Basu, U. (2009): Explicit finite element perfectly matched layer for transient three-dimensional elastic waves. *Int. J. Numer. Meth. Engng.*, vol. 77, pp. 151–176.

Basu, U.; Chopra, A. K. (2004): Perfectly matched layers for transient elastodynamics of unbounded domains. *Int. J. Numer. Meth. Engng.*, vol. 59, pp. 1039–1074.

Bécache, E.; Fauqueux, S.; Joly, P. (2003): Stability of perfectly matched layers, group velocities and anisotropic waves. *J. Comput. Phys.*, vol. 188, no. 2, pp. 399–433.

Bécache, E.; Joly, P. (2002): On the analysis of Bérenger's perfectly matched layers for Maxwell's equations. *M2AN*, vol. 36, no. 1, pp. 87–120.

Bérenger, J. P. (1994): A Perfectly Matched Layer for the absorption of electromagnetic waves. *J. Comput. Phys.*, vol. 114, pp. 185–200.

Bérenger, J. P. (2002): Application of the CFS PML to the absorption of evanescent waves in waveguides. *IEEE Microwave and Wireless Components Letters*, vol. 12, no. 6, pp. 218–220.

Bérenger, J. P. (2002): Numerical reflection from FDTD-PMLs: A comparison of the split PML with the unsplit and CFS PMLs. *IEEE Transactions on Antennas and Propagation*, vol. 50, no. 3, pp. 258–265.

Carcione, J. M. (1994): The wave equation in generalized coordinates. *Geophysics*, vol. 59, pp. 1911–1919.

Cerjan, C.; Kosloff, D.; Kosloff, R.; Reshef, M. (1985): A nonreflecting boundary condition for discrete acoustic and elastic wave equation. *Geophysics*, vol. 50, pp. 705–708.

Chew, W. C.; Liu, Q. (1996): Perfectly Matched Layers for elastodynamics: a new absorbing boundary condition. *J. Comput. Acoust.*, vol. 4, no. 4, pp. 341–359.

Chew, W. C.; Weedon, W. H. (1994): A 3-D perfectly matched medium from modified Maxwell's equations with stretched coordinates. *Microwave Opt. Technol. Lett.*, vol. 7, no. 13, pp. 599–604.

Clayton, R.; Engquist, B. (1977): Absorbing boundary conditions for acoustic and elastic wave equations. *Bull. Seismol. Soc. Am.*, vol. 67, pp. 1529–1540.

Cohen, G.; Fauqueux, S. (2005): Mixed spectral finite elements for the linear elasticity system in unbounded domains. *SIAM Journal on Scientific Computing*, vol. 26, no. 3, pp. 864–884.

Collino, F.; Monk, P. (1998): The Perfectly Matched Layer in curvilinear coordinates. *SIAM J. Sci. Comput.*, vol. 19, no. 6, pp. 2061–2090.

Collino, F.; Tsogka, C. (2001): Application of the PML absorbing layer model to the linear elastodynamic problem in anisotropic heterogeneous media. *Geophysics*, vol. 66, no. 1, pp. 294–307.

Dong, L.; She, D.; Guan, L.; Ma, Z. (2005): An eigenvalue decomposition method to construct absorbing boundary conditions for acoustic and elastic wave equations. *J. Geophys. Eng.*, vol. 2, pp. 192–198.

Drossaert, F. H.; Giannopoulos, A. (2007): A nonsplit complex frequency-shifted PML based on recursive integration for FDTD modeling of elastic waves. *Geophysics*, vol. 72, no. 2, pp. T9–T17.

Dumbser, M.; Käser, M. (2006): An arbitrary high-order discontinuous Galerkin method for elastic waves on unstructured meshes-II. The three-dimensional isotropic case. *Geophys. J. Int.*, vol. 167, no. 1, pp. 319–336.

Engquist, B.; Majda, A. (1977): Absorbing boundary conditions for the numerical simulation of waves. *Math. Comp.*, vol. 31, pp. 629–651.

Fauqueux, S. (2003): *Eléments finis mixtes spectraux et couches absorbantes parfaitement adaptées pour la propagation d'ondes élastiques en régime transitoire*. PhD thesis, Université Paris-Dauphine, France, 2003.

Festa, G.; Delavaud, E.; Vilotte, J. P. (2005): Interaction between surface waves and absorbing boundaries for wave propagation in geological basins: 2D numerical simulations. *Geophys. Res. Lett.*, vol. 32, no. 20, pp. L20306.

Festa, G.; Vilotte, J. P. (2005): The Newmark scheme as velocity-stress time-staggering: an efficient PML implementation for spectral-element simulations of elastodynamics. *Geophys. J. Int.*, vol. 161, pp. 789–812.

Gedney, S. D. (1998): The Perfectly Matched Layer absorbing medium. In Taflove, A.(Ed): *Advances in Computational Electrodynamics: the Finite-Difference Time-Domain method*, chapter 5, pp. 263–343. Artech House, Boston.

Gedney, S. D.; Zhao, B. (2009): An Auxiliary Differential Equation Formulation for the Complex-Frequency Shifted PML. *IEEE Transactions on Antennas and Propagation.* Submitted.

Givoli, D. (1991): Non-reflecting boundary conditions: review article. *J. Comput. Phys.*, vol. 94, pp. 1–29.

Givoli, D. (2004): High-order local non-reflecting boundary conditions: A review. *Wave Motion*, vol. 39, pp. 319–326.

Givoli, D. (2008): Computational absorbing boundaries. In Marburg, S.; Nolte, B.(Eds): *Computational Acoustics Noise Propagation in Fluids*, volume 5, pp. 145–166. Springer-Verlag, Berlin, Germany.

Grote, M. J. (2000): Nonreflecting boundary conditions for elastodynamics scattering. *J. Comput. Phys.*, vol. 161, pp. 331–353.

Guddati, M. N.; Lim, K. W. (2006): Continued fraction absorbing boundary conditions for convex polygonal domains. *Int. J. Numer. Meth. Engng.*, vol. 66, no. 6, pp. 949–977.

Hagstrom, T. (1999): Radiation boundary conditions for the numerical simulation of waves. *Acta Numerica*, vol. 8, pp. 47–106.

Hagstrom, T.; Hariharan, S. I. (1998): A formulation of asymptotic and exact boundary conditions using local operators. *Appl. Num. Math.*, vol. 27, pp. 403–416.

Higdon, R. L. (1991): Absorbing boundary conditions for elastic waves. *Geophysics*, vol. 56, pp. 231–241.

Hughes, T. J. R. (1987): *The finite element method, linear static and dynamic finite element analysis*. Prentice-Hall International, Englewood Cliffs, New Jersey, USA.

Kawase, H. (1988): Time-domain response of a semi-circular canyon for incident *SV*, *P* and Rayleigh waves calculated by the discrete wavenumber boundary element method. *Bull. Seismol. Soc. Am.*, vol. 78, pp. 1415–1437.

Komatitsch, D.; Martin, R. (2007): An unsplit convolutional Perfectly Matched Layer improved at grazing incidence for the seismic wave equation. *Geophysics*, vol. 72, no. 5, pp. SM155–SM167.

Komatitsch, D.; Martin, R.; Tromp, J.; Taylor, M. A.; Wingate, B. A. (2001): Wave propagation in 2-D elastic media using a spectral element method with triangles and quadrangles. *J. Comput. Acoust.*, vol. 9, no. 2, pp. 703–718.

Komatitsch, D.; Tromp, J. (1999): Introduction to the spectral-element method for 3-D seismic wave propagation. *Geophys. J. Int.*, vol. 139, no. 3, pp. 806–822.

Komatitsch, D.; Tromp, J. (2003): A Perfectly Matched Layer absorbing boundary condition for the second-order seismic wave equation. *Geophys. J. Int.*, vol. 154, no. 1, pp. 146–153.

Komatitsch, D.; Vilotte, J. P. (1998): The spectral-element method: an efficient tool to simulate the seismic response of 2D and 3D geological structures. *Bull. Seismol. Soc. Am.*, vol. 88, no. 2, pp. 368–392.

Kuzuoglu, M.; Mittra, R. (1996): Frequency dependence of the constitutive parameters of causal perfectly matched anisotropic absorbers. *IEEE Microwave and Guided Wave Letters*, vol. 6, no. 12, pp. 447–449.

Lu, Y. Y.; Zhu, J. (2007): Perfectly matched layer for acoustic waveguide modeling - Benchmark calculations and perturbation analysis. *CMES: Computer Modeling in Engineering & Sciences*, vol. 22, no. 3, pp. 235–248.

Luebbers, R. J.; Hunsberger, F. (1992): FDTD for Nth-order dispersive media. *IEEE Transactions on Antennas and Propagation*, vol. 40, no. 11, pp. 1297–1301.

Lysmer, J.; Drake, L. A. (1972): A finite element method for seismology. In *Methods in Computational Physics*, volume 11. Academic Press, New York, USA.

Ma, S.; Liu, P. (2006): Modeling of the perfectly matched layer absorbing boundaries and intrinsic attenuation in explicit finite-element methods. *Bull. Seismol. Soc. Am.*, vol. 96, no. 5, pp. 1779–1794.

Madariaga, R. (1976): Dynamics of an expanding circular fault. *Bull. Seismol. Soc. Am.*, vol. 66, no. 3, pp. 639–666.

Martin, R.; Komatitsch, D.; Blitz, C.; Le Goff, N. (2008): Simulation of seismic wave propagation in an asteroid based upon an unstructured MPI spectral-element method: blocking and non-blocking communication strategies. *Lecture Notes in Computer Science*, vol. 5336, pp. 350–363.

Martin, R.; Komatitsch, D.; Ezziani, A. (2008): An unsplit convolutional Perfectly Matched Layer improved at grazing incidence for seismic wave equation in poroelastic media. *Geophysics*, vol. 73, no. 4, pp. T51–T61.

Meza-Fajardo, K. C.; Papageorgiou, A. S. (2008): A nonconvolutional, split-field, perfectly matched layer for wave propagation in isotropic and anisotropic elastic media; stability analysis. *Bull. Seismol. Soc. Am.*, vol. 98, no. 4, pp. 1811–1836.

Moczo, P.; Kristek, J.; Bystrický, E. (2001): Efficiency and optimization of the 3-D finite-difference modeling of seismic ground motion. *J. Comput. Acoust.*, vol. 9, no. 2, pp. 593–609.

Nissen-Meyer, T.; Fournier, A.; Dahlen, F. A. (2008): A 2-D spectral-element method for computing spherical-earth seismograms - II. Waves in solid-fluid media. *Geophys. J. Int.*, vol. 174, pp. 873–888.

Peng, C. B.; Töksoz, M. N. (1995): An optimal absorbing boundary condition for elastic wave modeling. *Geophysics*, vol. 60, pp. 296–301.

Roden, J. A.; Gedney, S. D. (2000): Convolution PML (CPML): An efficient FDTD implementation of the CFS-PML for arbitrary media. *Microwave and Optical Technology Letters*, vol. 27, no. 5, pp. 334–339.

Rodríguez-Castellanos, A.; Sánchez-Sesma, F.; Luzón, F.; Martin, R. (2006): Multiple scattering of elastic waves by subsurface fractures and cavities. *Bull. Seismol. Soc. Am.*, vol. 96, no. 4A, pp. 1359–1374.

Sánchez-Sesma, F. J.; Campillo, M. (1991): Diffraction of *P*, *SV* and Rayleigh waves by topographic features: a boundary integral formulation. *Bull. Seismol. Soc. Am.*, vol. 81, pp. 2234–2253.

Simo, J. C.; Tarnow, N.; Wong, K. K. (1992): Exact energy-momentum conserving algorithms and symplectic schemes for nonlinear dynamics. *Comput. Methods Appl. Mech. Engrg.*, vol. 100, pp. 63–116.

Soares-Jr, D.; Mansur, W. J.; Lima, D. L. (2007): An explicit multi-level time-step algorithm to model the propagation of interacting acoustic-elastic waves using finite-element/finite-difference coupled procedures. *CMES: Computer Modeling in Engineering & Sciences*, vol. 17, no. 1, pp. 19–34.

Sochacki, J.; Kubichek, R.; George, J.; Fletcher, W. R.; Smithson, S. (1987): Absorbing boundary conditions and surface waves. *Geophysics*, vol. 52, no. 1, pp. 60–71.

Stacey, R. (1988): Improved transparent boundary formulations for the elastic wave equation. *Bull. Seismol. Soc. Am.*, vol. 78, no. 6, pp. 2089–2097.

Tessmer, E.; Kosloff, D. (1994): 3-D elastic modeling with surface topography by a Chebyshev spectral method. *Geophysics*, vol. 59, no. 3, pp. 464–473.

Virieux, J. (1986): *P-SV* wave propagation in heterogeneous media: velocity-stress finite-difference method. *Geophysics*, vol. 51, pp. 889–901.

Zeng, Y. Q.; He, J. Q.; Liu, Q. H. (2001): The application of the perfectly matched layer in numerical modeling of wave propagation in poroelastic media. *Geophysics*, vol. 66, no. 4, pp. 1258–1266.